Surface & Coatings Technology 369 (2019) 16–30

Contents lists available at ScienceDirect

Surface & Coatings Technology

journal homepage: www.elsevier.com/locate/surfcoat

Influences of plasma arc remelting on microstructure and service performance of Cr_3C_2-NiCr/NiCrAl composite coating

Ji-yu Du, Fang-yi Li*, Yan-le Li*, Li-ming Wang, Hai-yang Lu, Xue-ju Ran, Xing-yi Zhang

[a] Key Laboratory of High Efficiency and Clean Mechanical Manufacture, Ministry of Education, School of Mechanical Engineering, Shandong University, Jinan 250061, China

[b] National Demonstration Center for Experimental Mechanical Engineering Education, Shandong University, Jinan 250061, China

ARTICLE INFO

Keywords:
Cr_3C_2-NiCr/NiCrAl composite coating
Plasma arc remelting
Adhesion
Microhardness
Sliding wear resistance

ABSTRACT

This work studies the influences of plasma arc remelting on the microstructure and properties of thermal sprayed Cr_3C_2-NiCr/NiCrAl composite coating. The microstructure and composition are analyzed by scanning electron microscope (SEM) and X-ray diffraction (XRD). The microstructure and density of the coating are modified after remelting. It is found that the amounts of the $Cr_{23}C_6$ and Cr_2O_3 phases of the remelted coating are increased compared with the as-sprayed coating. Based on the experimental results, the coating adhesion, microhardness and wear resistance are all enhanced through plasma arc remelting with limited power (below 42 kW). Specifically, the adhesion is improved due to the enhancement of the element diffusion near the interface and metallurgical bonding between the functional and bonding layer. In addition, the increase of microhardness is attributed to the decrease of porosity and the formation of secondary carbides and eta phase. However, remelting with excessive powers (above 42 kW) results in the delamination of the mechanical joint between the bonding layer and substrate, which has adverse effect on coating adhesion as well as the wear resistance. Therefore, the proper usage of plasma arc remelting is an effective approach to enhance the properties of the thermal sprayed Cr_3C_2-NiCr/NiCrAl composite coating.

1. Introduction

Chromium carbide has been widely used as one of the metal carbides due to its high hardness, high melting point, high elastic modulus, great chemical corrosion resistance and wear resistance [1,2]. The thermal sprayed Cr_3C_2-NiCr has been successfully applied for surface protection and modification in the fields of aerospace, automobile, energy, etc. due to high temperature wear resistance, corrosion resistance and high hardness [3–6]. The chromium carbide coatings provide excellent resistance to high-temperature oxidation (up to 750 °C) and reduce the decrease in the coating properties such as wear resistance and hardness due to the formation of the Cr_2O_3 on its surface [7]. Therefore, high-temperature wear protection applications are served by chromium carbide based hardmetals, mainly Cr_3C_2-NiCr with 20–25 wt% binder phase [8]. Among various thermal spray technologies, high velocity oxy-fuel (HVOF) offers excellent micro hardness, good adhesion between splats and minimum porosity of the coated specimens [9–11]. Nowadays, Cr_3C_2-NiCr is almost exclusively deposited by means of high velocity oxygen-fuel (HVOF) spraying [12].

A heterogeneous interface usually exists between a thermal spray coating and its substrate, since the adhesion of a thermal spray coating to the substrate is mainly mechanical. Poor inter-lamellar contact is caused by the presence of porosity and microcracks in the sprayed coating, which affects bonding strength and hardness [13,14]. Post heat treatment of the coating is one of the methods to solve those problems and improve the service properties of HVOF sprayed coatings. The heat treatment has positive effect on coating quality and performance and eliminates defects and imperfections of the coatings. After the heat treatment process, the properties of the Cr_3C_2-NiCr coating can be enhanced to improve the erosion resistance. Carbide dissolution has an important role in governing the hardness and the phases present in the coating [15–17].

Carbide dissolution has a critical impact on the binder hardness, and the super saturation of the NiCr binder matrix makes it prone to brittle cracking. Other factors such as inter-splat adhesion, splat size, level of porosity and cracks, and the presence of oxide stringers also have a significant effect on the erosion behavior [5]. Iiszko and Nitkiewicz [18] proposed that the remelting treatment revealed a significant

* Corresponding authors at: Key Laboratory of High Efficiency and Clean Mechanical Manufacture, Ministry of Education, School of Mechanical Engineering, Shandong University, Jinan 250061, China.

E-mail addresses: lifangyi@sdu.edu.cn (F.-y. Li), yanle.li@sdu.edu.cn (Y.-l. Li).

https://doi.org/10.1016/j.surfcoat.2019.04.037
Received 4 December 2018; Received in revised form 8 April 2019; Accepted 9 April 2019
Available online 11 April 2019

Table 1
The characteristics of Cr_3C_2-NiCr and NiCrAl powder.

Powder material	Grade	Chemical composition	Morphology	Particle diameter μm
Cr_3C_2-NiCr	GP25NC	75%Cr3C2; 25%NiCr	Spherical	−45/+15
NiCrAl	ZX.NiCrAl	4.5–6.5%Al; 18–20%Cr; Ni balance	Spherical	−48/+25

reduction of porosity (both open and closed ones), homogenization of the chemical composition, smoothing of the surface, and improvement of coating adhesion to the substrate. Heat treatment in inert atmosphere and vacuum significantly improve wear resistance and reduce residual stress of WC-Co and Cr_3C_2-NiCr coatings [19–21]. Janka et al. [22] concluded that post spraying heat treatments in a temperature range of 400–800 °C strongly improves the high-stress sliding wear resistance of Cr_3C_2-NiCr coatings, and the hardness of heat treated Cr_3C_2-NiCr coating increased due to the precipitation hardening effect at 600 °C and decreased at 800 °C due to Orowan bowing process as particle by-passing mechanism of dislocation migration. Morimoto et al. [23] found that the average hardness of laser-treated Cr_3C_2–25%NiCr cermet coatings is higher than that of HVOF coatings and laser remelting markedly improved the wear resistance of HVOF sprayed Cr_3C_2–25% NiCr cermet coatings.

Different post-spraying treatment processes such as heat treatment in furnace, flame treatment and laser irradiation can be used. However, heat treatment in furnace requires to heat both the coating and substrate, which has adverse effects on the substrate. Flame heating easily leads to uneven heating, which results in deformation and cracks in the coating. Due to the large differences of the thermal expansion coefficient, elastic modulus and thermal conductivity between ceramic materials and metallic substrates, laser treatment may induce a high number of microcracks that are generated by the thermal stress induced by the rapid heating and cooling rates. Furthermore, the laser treatment is more expensive [24].

Unlike the above post-spraying treatment methods, the plasma arc remelting is based on using a plasma arc, which is a kind of concentrated arc with high energy density and extremely high temperature. The temperature at the exit of the plasma nozzle is over 10,000 °C and the plasma arc has been widely used in traditional metallurgical processes, such as plasma spray, plasma welding, plasma cutting, etc. [25–27]. During plasma arc remelting, the arc energy is concentrated and controllable, thus oxidation can be inhibited by inert gas protection. In addition, in-situ remelting can be carried out and the production efficiency is improved due to the simplified operation process. Plasma arc remelting is a more convenient and effective post-spraying treatment method compared with other methods.

Xie et al. [28] suggested that a denser microstructure can be obtained by plasma arc remelting of a plasma-sprayed Cr3C2-NiCr coating, and remelting enhances the microhardness and corrosion resistance of the coating. Complementary to this approach, in this paper, plasma arc remelting is conducted on the thermal sprayed Cr_3C_2-NiCr/NiCrAl coating. The objective of the present investigation is to study the influence of remelting power on the microstructure and properties of the coatings. Section 2 describes the experimental details including microstructure and phase composition characterization, measurement of bonding strength and hardness, and the evaluation of porosity and wear resistance. Microstructure and microhardness of remelted coatings are analyzed to study the influence of remelting power on the density. Bonding strength and interface of remelted coatings are investigated to study the influence of remelting power on coating adhesion, and the mechanism for the enhancement of bonding strength is studied by analyzing element diffusion across the interface. Friction coefficient and wear rate of coatings remelted with different arc power settings are explored.

2. Experimental details

2.1. Coating deposition

The NiCrAl bonding layer was prepared on the martensitic, precipitation hardening stainless steel FV520B substrate which is widely used for large centrifugal compressors impeller blade. The workpiece was grit-blasted with brown corundum sand (24 mesh) after ultrasonic cleaning. The inlet pressure is 0.7 MPa and the blasting angle is 90°. The blasting distance is 100 mm and the surface roughness is approximately Ra 8.43 μm after grit blasting. The workpiece is cleaned ultrasonically by using acetone before spraying, the cleaning time is set as 10 min. The workpiece is subsequently dried. The Cr_3C_2-NiCr functional layer was then prepared on the bonding layer by using the XM-5000 HVOF system. Propane was used as fuel, with pure oxygen used as comburent. Meanwhile the powder was delivered in the axial direction. The characteristics of the NiCrAl powder from Zhenxing Metals company (ZXC) and Cr_3C_2-NiCr powder from Golden Egret Geotools company (XTC) are shown in Table 1. The adopted spraying process parameters during the spraying process are shown in Tables 2 and 3. Then, Cr_3C_2-NiCr/NiCrAl coating was remelted by using XM-80jz plasma gun. The argon and gas shields were used to suppress coating oxidation during remelting, and the input argon pressure of shielding gas is 0.1 MPa. The remelting powers ranged from 30 kW to 45 kW by adjusting the spray voltage and current. The parameters during the remelting process are set as shown

Table 2
Process parameters of plasma spraying NiCrAl coating.

Powder material	Spray voltage V	Spray current A	Spray distance mm	Main gas flow rate L/H	Argon pressure MPa	Nitrogen pressure MPa	Spray speed m/min	Spray interval mm	Rotating dish speed r/min
NiCrAl	65	550	120	1800	0.8	0.72	2	4	0.8

Table 3
Process parameters of supersonic flame spraying Cr_3C_2-NiCr coating.

Powder material	Oxygen pressure MPa	Oxygen flow m^3/h	Propane pressure MPa	Propane flow m^3/h	Hydrogen pressure MPa	Nitrogen pressure MPa	Spray span mm	Spray interval mm	Spray speed m/min	Rotating dish speed r/min
Cr_3C_2-NiCr	1.3	80	0.7	40	0.3	1.2	180	4	2	2.5

Table 4
Parameters during the remelting process.

Sample	Power kW	Distance mm	Speed m/min
RP30	30	50	0.2
RP33	33	50	0.2
RP36	36	50	0.2
RP39	39	50	0.2
RP42	42	50	0.2
RP45	45	50	0.2

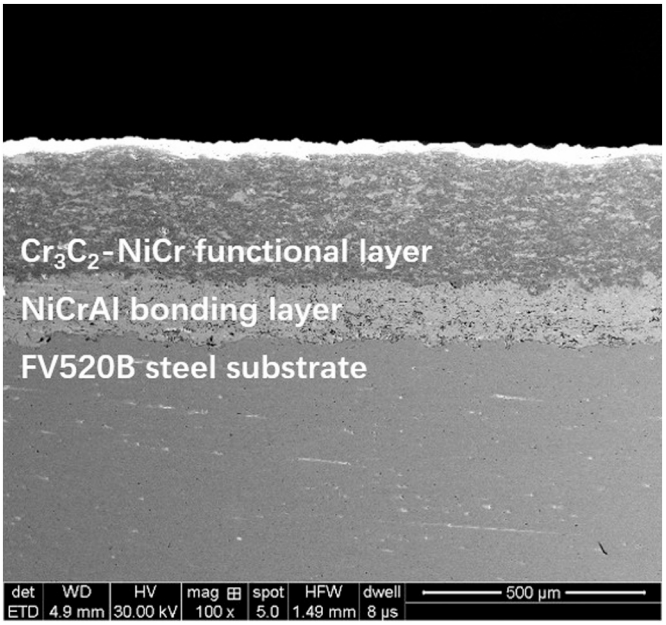

Fig. 1. The SEM micrograph of the cross-section for the as-sprayed coating.

in Table 4.

2.2. Microstructure characterization

The cross-sections of coatings remelted at various powder levels were ground and polished for microstructure characterization. The microstructure was examined by a QUANTA FEG 250 scanning electron microscope (SEM) with a back-scattered electron detector (BSE-mode). The element composition of the prepared samples was analyzed by an INCA Energy X-MAX-50 energy dispersive spectrometer.

2.3. Phase composition characterization

The phase composition of the coating was tested by a Rigaku DMAX-2500PC X-ray diffractometer, in which the diffraction angle is between 20 and 90°. The results were then analyzed by using the MDI Jade software. The measured samples were compared with the PDF standard cards as the reference to retrieve all the phases in the samples.

2.4. Adhesion measurement

The bonding strength between the coating and substrate was measured according to ASTM-C633 standard. Five cylindrical specimens were covered with the Cr_3C_2-NiCr/NiCrAl coating in each experiment, and bonded with other counter-specimens by an adhesive with the axis lines of specimens coincident. The used adhesive was E-7, manufactured by Huayi, and specimens were kept at 120 °C for 3 h for solidification. The Instron 8801 testing machine was used for tensile tests.

2.5. Microhardness testing

Microhardness values of the coatings surfaces and cross-sections were checked with a MH-6 Vickers indenter. A preload of 300 g was held for 5 s. The measurements were performed on the coating cross-section from the coating-substrate interface to the coating surface. For each test, the highest and lowest values were discarded among the 10 measurements, then the average of the remaining values was calculated

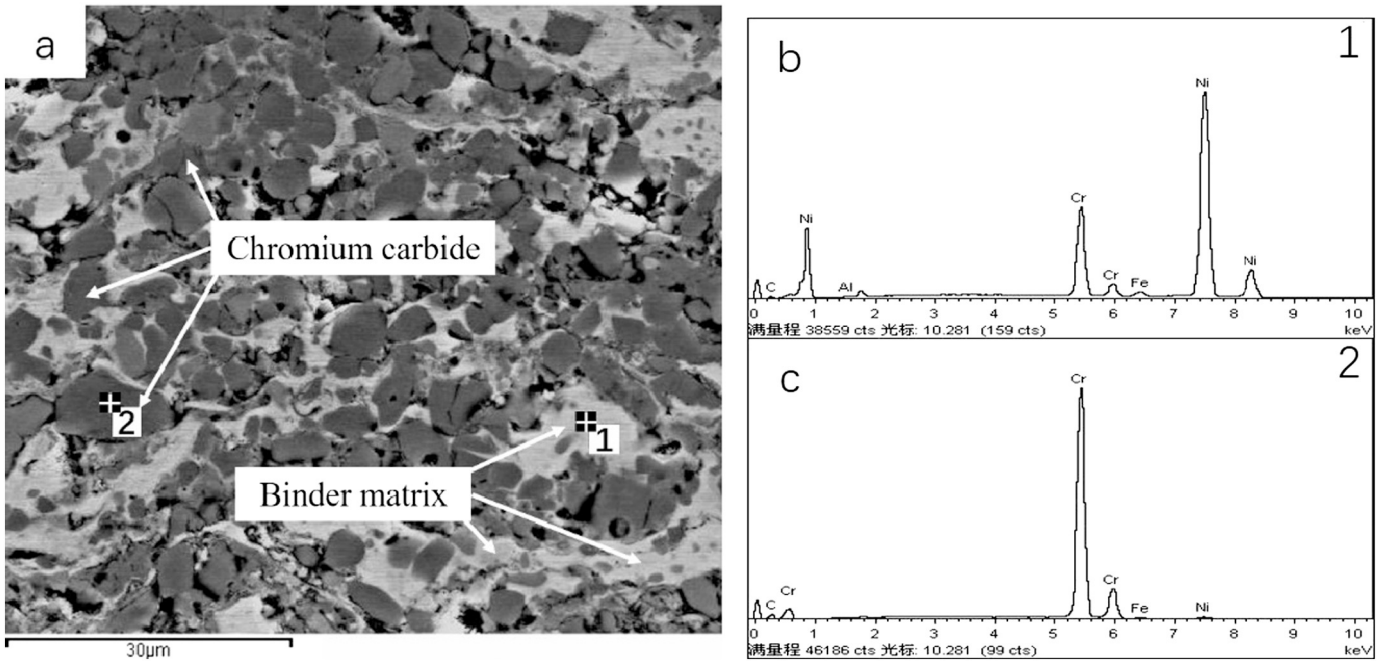

Fig. 2. The SEM micrograph and EDS spectra of the Cr_3C_2-NiCr functional layer: (a) location of point 1 and point 2, (b) EDS spectrum of point 1, (c) EDS spectrum of point 2.

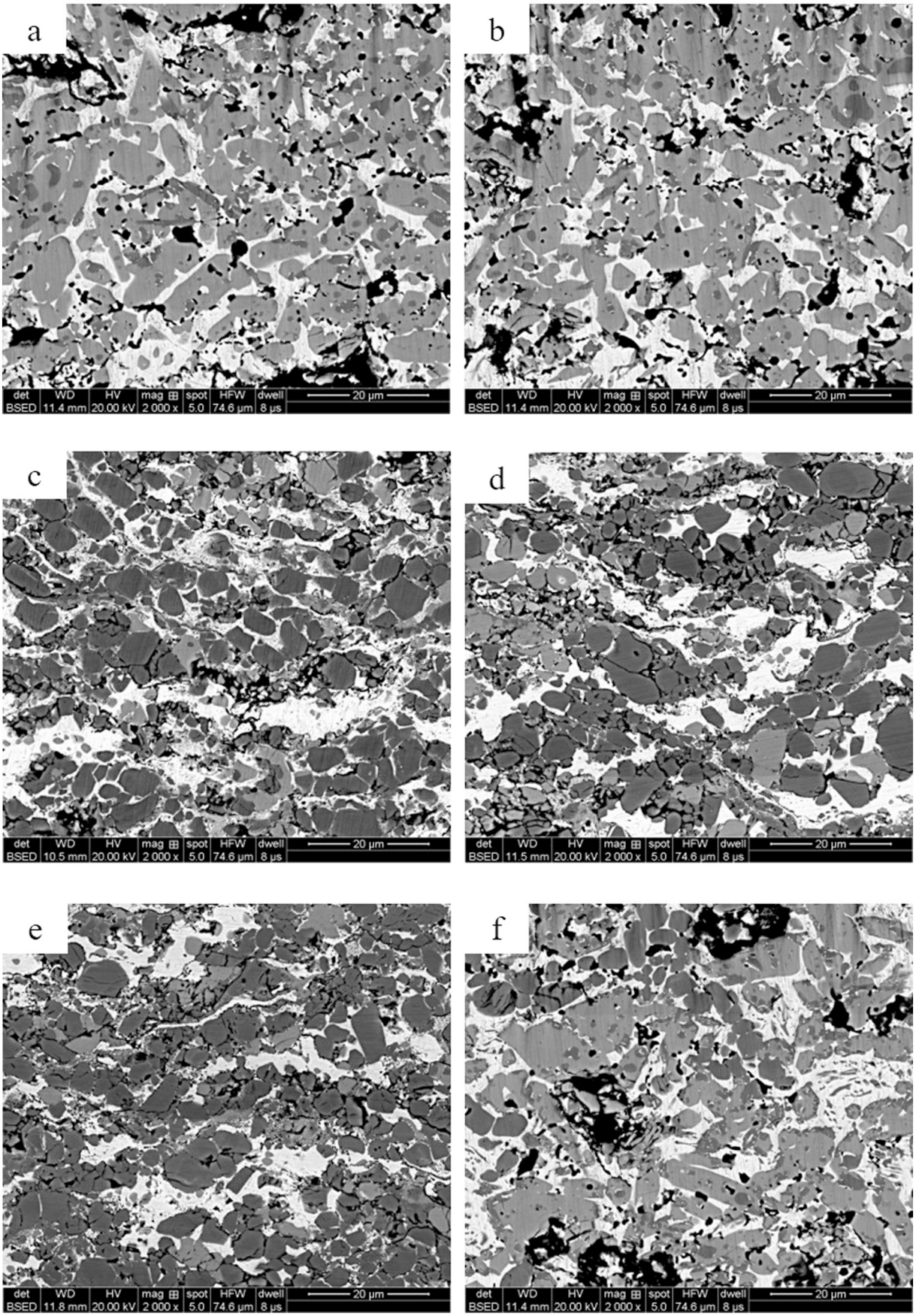

Fig. 3. Microstructure of Cr_3C_2-NiCr functional layer after plasma remelting: (a) Plasma remelting at 30 kW (RP30), (b) Plasma remelting at 33 kW (RP33), (c) Plasma remelting at 36 kW (RP36), (d) Plasma remelting at 39 kW (RP39), (e) Plasma remelting at 42 kW (RP42) (f) Plasma remelting at 45 kW (RP45).

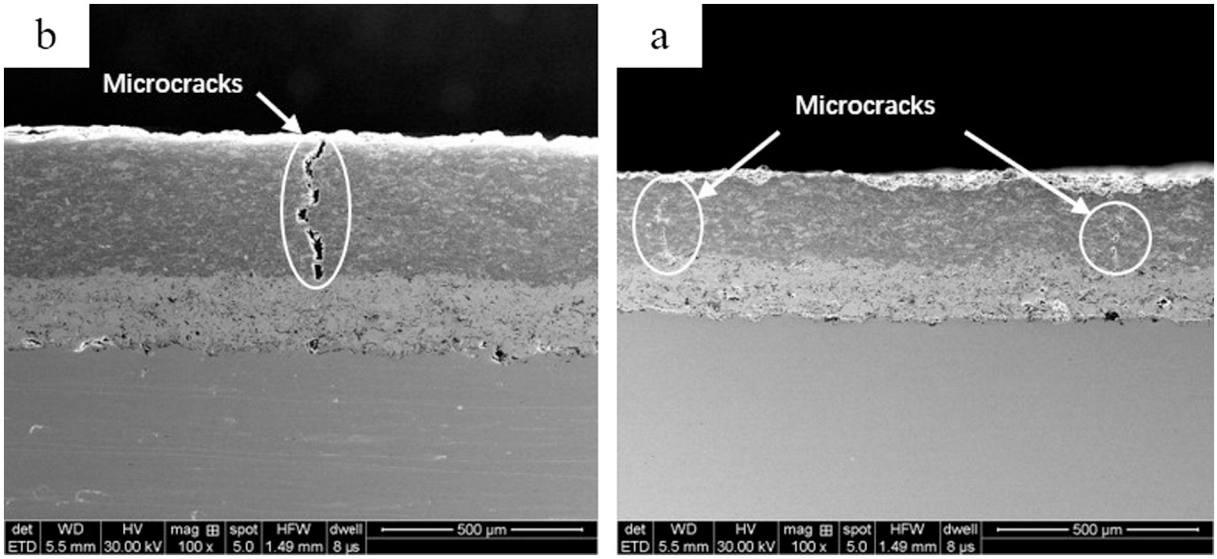

Fig. 4. Grid-like cracks in the RP45 coating.

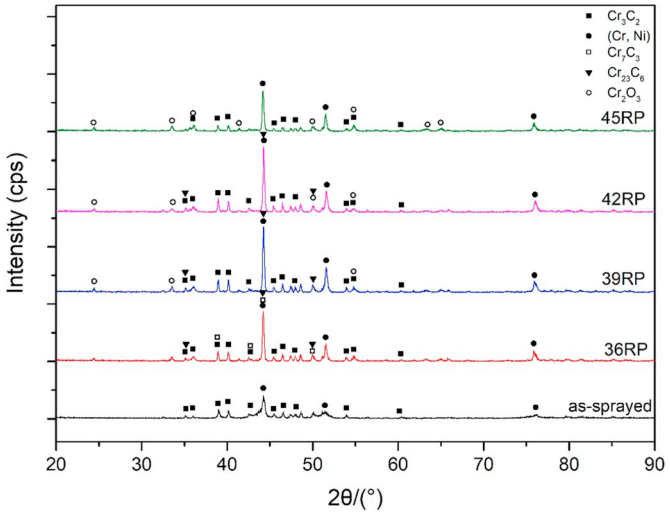

Fig. 5. X-ray diffraction patterns of Cr_3C_2-NiCr functional layer after plasma remelting.

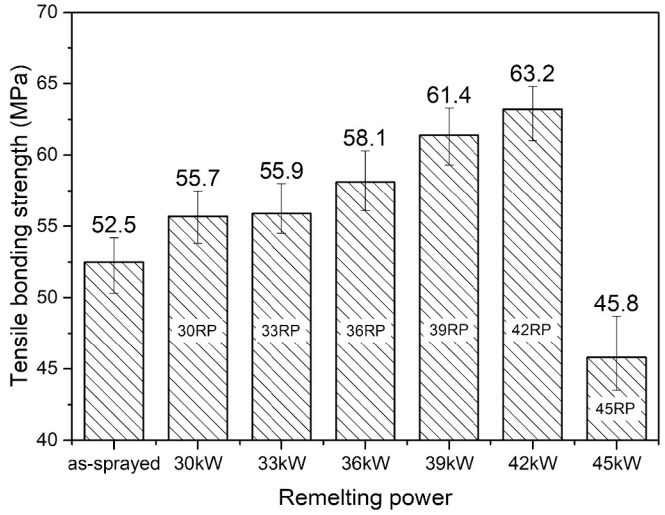

Fig. 6. Tensile bonding strength of plasma remelted coatings.

as the microhardness of the coatings.

2.6. Porosity testing

Defects such as pores and cracks can be found in layers deposited by thermal spraying technology. Porosity is an important index to measure the density of the deposited layer, and it would affect its quality and service performance. SEM image analysis was used to measure the porosity of the coating. Magnification factors between 500 and 1000 of secondary electron maps were selected. The Image J software was used to adjust gray scale and to determine the threshold between black and white areas according to coating microstructure. Then, the proportion of black areas was calculated and the coating porosity value was obtained. Nevertheless, the value measured by this method is slightly larger than the actual value of porosity.

2.7. Wear testing

The friction coefficient of the coating was determined by using the CETR UMT-2 friction and wear tester. The surface polishing treatment was performed before the wear test to ensure the surface roughness was less than Ra 0.8 µm. A GCr15 steel ball with a diameter of 9.525 mm was selected as the counterface, and point contact reciprocating motion under standard temperature conditions (25 °C) was selected. Five samples were tested for each remelting type and the test condition was dry friction. The parameters of friction and wear experiments are given in Table 3.

3. Results and discussions

3.1. Coating microstructure & phase composition

Fig. 1 shows the SEM image of the as-sprayed Cr_3C_2-NiCr/NiCrAl coating, which is comprised of Cr_3C_2-NiCr functional layer on the top, NiCrAl bonding layer in the middle and FV520B steel substrate in the bottom. Fig. 2 shows the EDS spectra of the Cr_3C_2-NiCr functional layer and Fig. 2a is the backscattered electrons image (BSE). It is observed that the layer is characterized by a significant amount of Chromium carbide particles entrained in the NiCr binder matrix, which is evident in the dark blocky particles and light gray filler [29]. The molten droplets hit the surface of the substrate and quickly cooled. During the

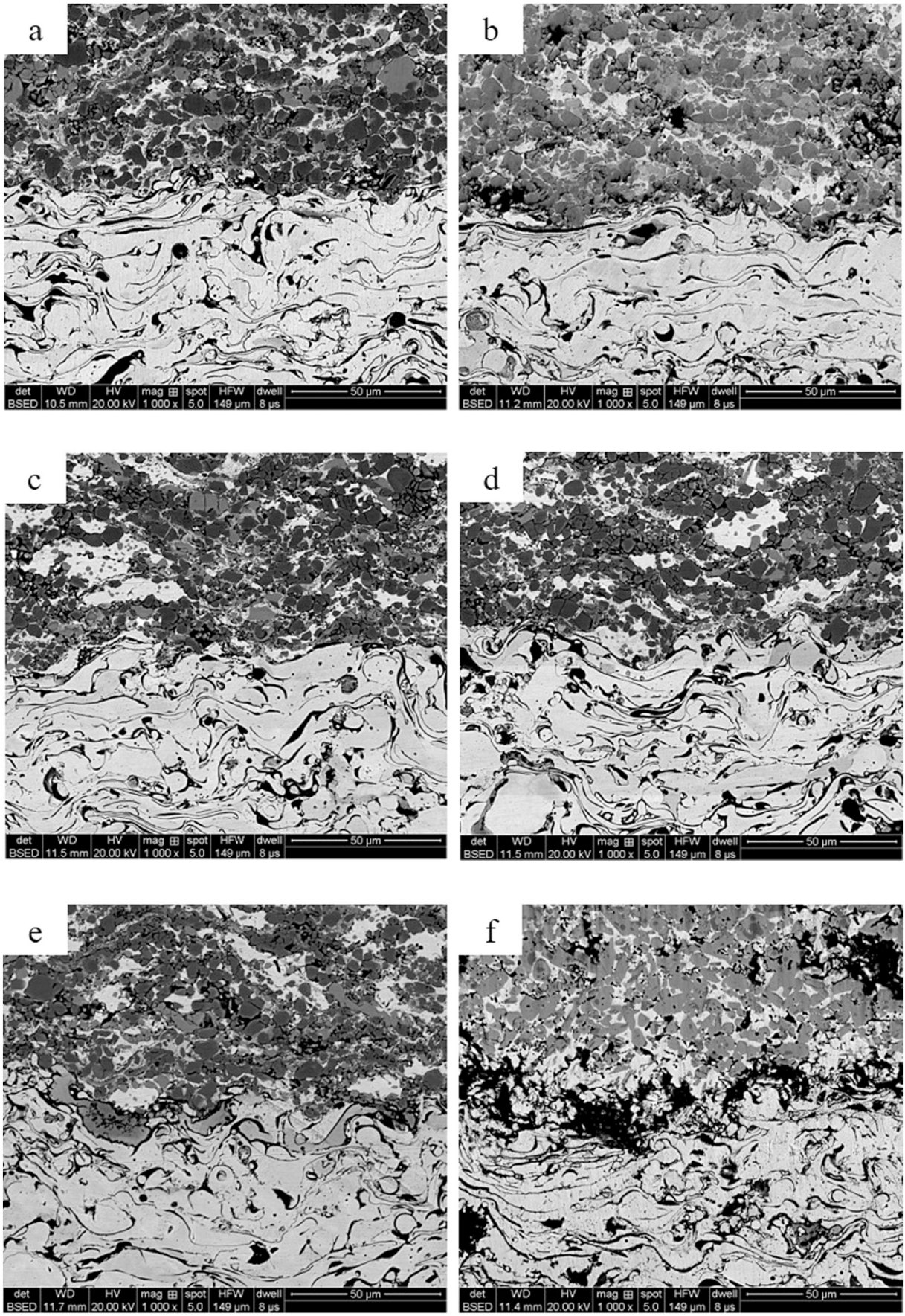

Fig. 7. Functional-bonding layer interface of coatings remelted at different powers: (a) Remelting power at 30 kW (RP30), (b) Remelting power at 33 kW (RP33), (c) Remelting power at 36 kW (RP36), (d) Remelting power at 39 kW (RP39), (e) Remelting power at 42 kW (RP42), (f) Remelting power at 45 kW (RP45).

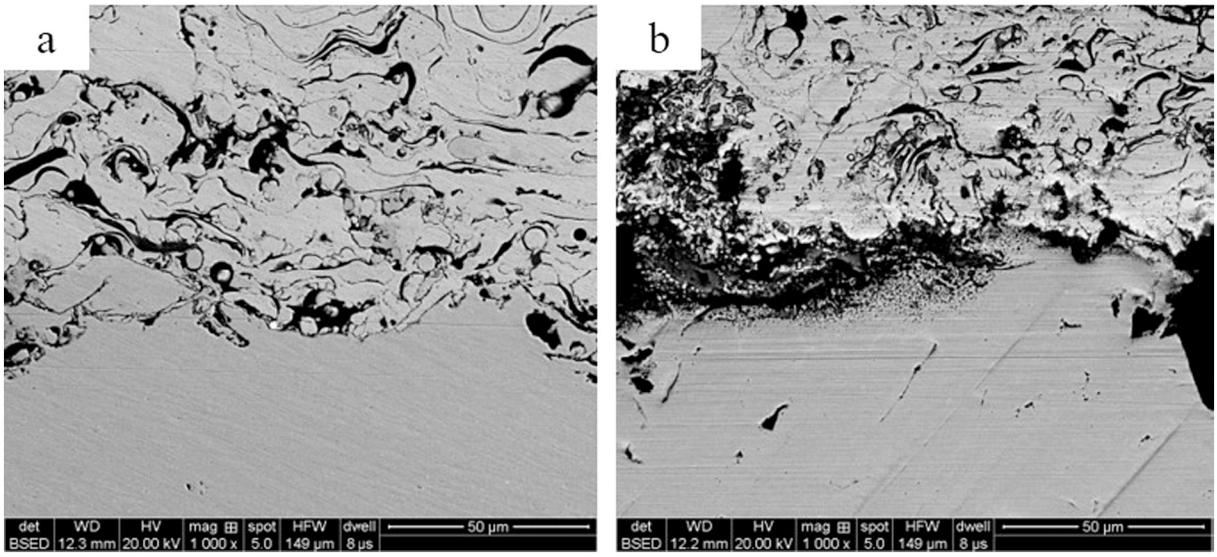

Fig. 8. Bonding layer-substrate interface of plasma-remelted coatings: (a) Plasma remelting at 36 kW (RP36), (b) Plasma remelting at 45 kW (RP45).

process, the NiCr metal in the molten droplets has no time to fill the gaps between the massive ceramic particles of Chromium carbide, which leads to the generation of porosity in the functional layer. The porosity is mostly concentrated in carbide cluster regions or splat boundaries [22], as shown in Fig. 2(a).

The influence of plasma remelting on the microstructure of the Cr_3C_2-NiCr functional layer is demonstrated in Fig. 3, and RP refers to remelting power. Compared with the as-sprayed coating, the microstructure change of RP30 layer and RP33 layer is not obvious according to Fig. 3(a) and (b). The reason is that the thermal input of plasma remelting at these conditions is not high enough to fully remelt the NiCr metal phase of the functional layer. By contrast, as shown in Fig. 3(c) and (d), the porosity of coating layers for RP36 and RP39 are decreased and the NiCr metallic phase distribution is more homogeneous. This is due to the fact that the remelting of NiCr metallic phase leads to the filling of the porosity and microcracks, resulting in the reduction of the quantity and dimension of porosity and microcracks in the functional layer. Noticeably, as the remelting power increases, the amounts of porosity and microcracks reach the minimum condition for the RP42 layer, as illustrated in Fig. 3(e). Nevertheless, when the remelting power is further increased to 45 kW, grid-like cracks can be observed on the layer surface, which extend to the bond layer, as shown in Fig. 4. It is found that the cracks and pores inside the functional layer increased significantly, resulting in the increase of porosity and the decrease of the density of the coating, as shown in Fig. 3(f).

Since the phase transformation for RP30 and RP33 coatings is not evident compared with that obtained at higher powers, only RP39, RP42 and RP45 coatings were selected for XRD analysis. As shown in Fig. 5, the main constituents of the remelted coatings are Cr_3C_2, (Cr, Ni), Cr_7C_3, Cr_2O_3 and $Cr_{23}C_6$. In particular, the amounts of $Cr_{23}C_6$ and Cr_2O_3 phases in the remelted coatings are increased compared with the original coating [30,31]. The following chemical reactions occur during the remelting process:

$$4Cr_3C_2 + 13O_2 \rightarrow 6Cr_{23}C_6 + 8CO(g) \quad (1)$$

$$4Cr + 3O_2 \rightarrow 2Cr_2O_3 \quad (2)$$

It can be seen from Fig. 4 that a trace amount of the Cr_2O_3 phase appears in the remelted coatings. However, as the remelting power increases from 42 kW to 45 kW, the content of $Cr_{23}C_6$ phase is decreased while the content of Cr_2O_3 phase is increased. When the remelting power increases from 39 kW to 45 kW, the oxidation phenomenon of the coating surface is more pronounced. This is because the coating surface is more easily oxidized at higher temperature when the plasma arc leaves, although the remelting process is protected by the inert gas argon.

3.2. Coating-substrate adhesion

As shown in Fig. 6, as the remelting power increases, the tensile bonding strength of the coating increases first and then sharply decreases. The tensile bonding strength of the RP42 layer peaks at 63.2 MPa. In the failure process, fracture of the coating often happens near the interface, especially the interface between functional and bonding layer. The reasons for the variation of tensile bonding strength of the Cr_3C_2-NiCr/NiCrAl coatings are investigated by analyzing the micromorphology and diffusion mechanism.

The coating contains two bonding interfaces: that between functional layer and bonding layer, and the one between bonding layer and substrate. Scanning electron microscopy was used to observe the microstructure of bonding interfaces under different remelting powers. The interface between functional layer and bonding layer is shown in Fig. 7, and the interface between bonding layer and matrix is shown in Fig. 8.

It can be seen from Fig. 7 that for RP30, RP33 and RP36 coatings, the boundaries between functional layer and bonding layer are relatively clear, and a considerable amount of pores and cracks can be observed near the interfaces between the two layers. As the remelting power increases to 39 kW and 42 kW, the interfaces between functional layer and bond layer are compact, and pores and cracks are reduced. As a result, the boundaries of the interface are blurred. Nevertheless, with the further increase of remelting power, especially in RP45, although the dispersion of nickel chrome metal component is more homogeneous across the interface between the functional layer and bonding layer, transverse cracks and pores occurred near the interface. Specifically, cracks grow and expand along the pores, which weakens the interface between the two layers, and degrades the service performance.

The interface between the bonding layer and substrate is shown in Fig. 8. With the remelting power of 36 kW (Fig. 8(a)), the bonding layer combined relatively well with the rough surface of the substrate. The

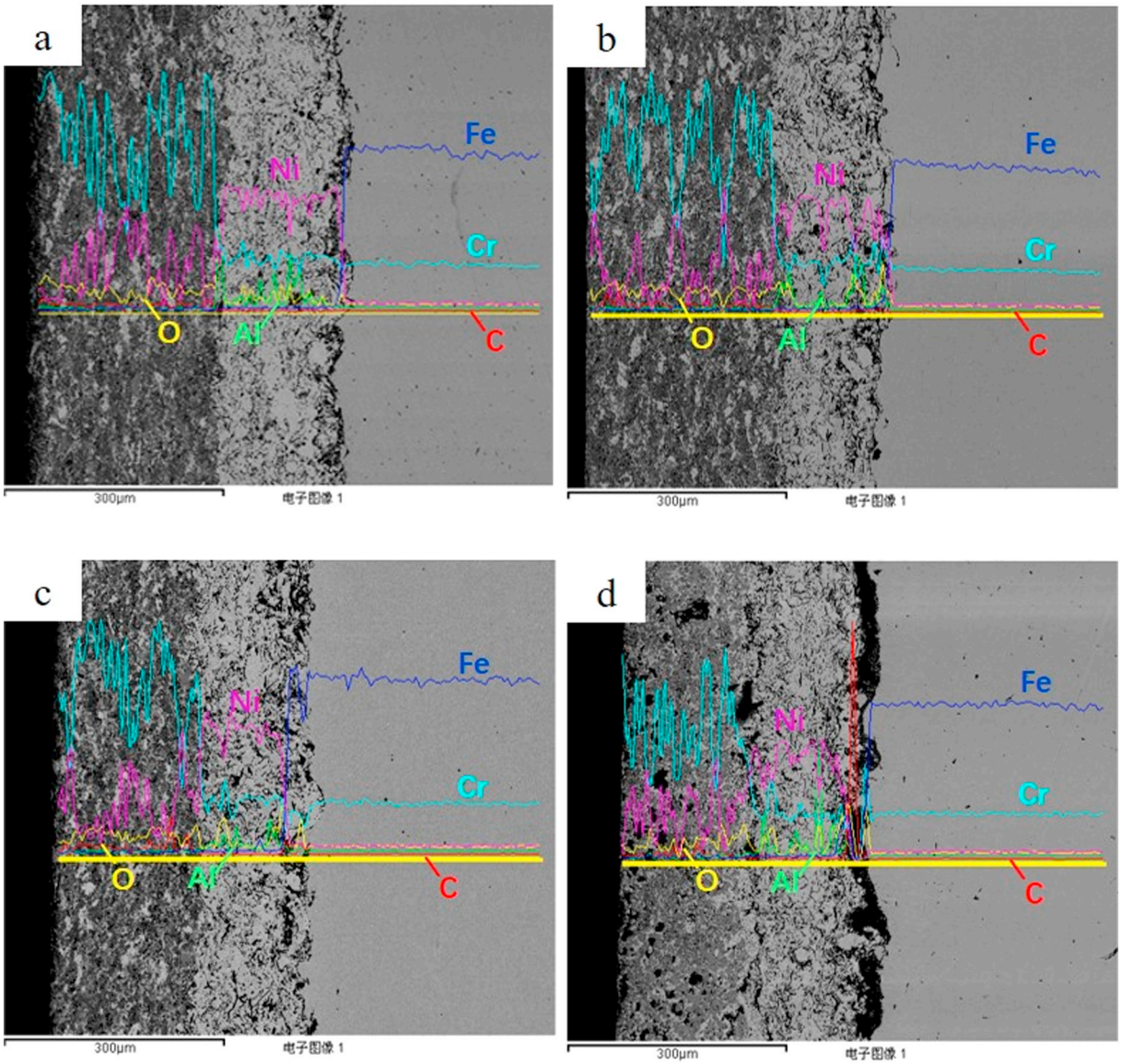

Fig. 9. EDS line scanning of remelted coatings: (a) Plasma remelting at 36 kW (RP36), (b) Plasma remelting at 39 kW (RP39), (c) Plasma remelting at 42 kW (RP42), (d) Plasma remelting at 45 kW (RP45).

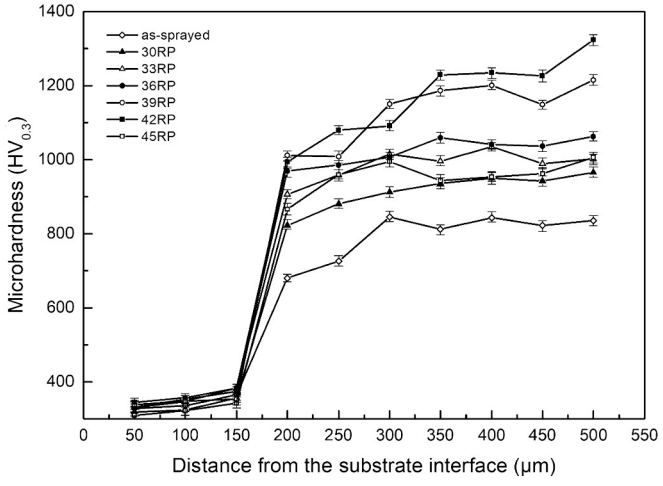

Fig. 10. Depth profile of coating microhardness.

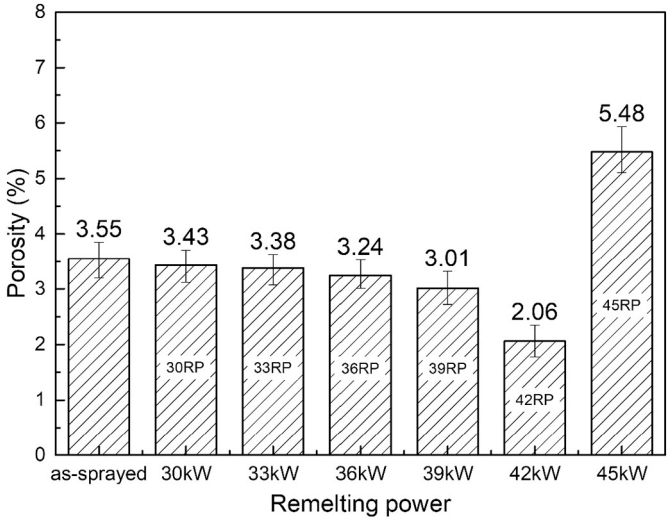

Fig. 11. Porosity of plasma remelted coatings.

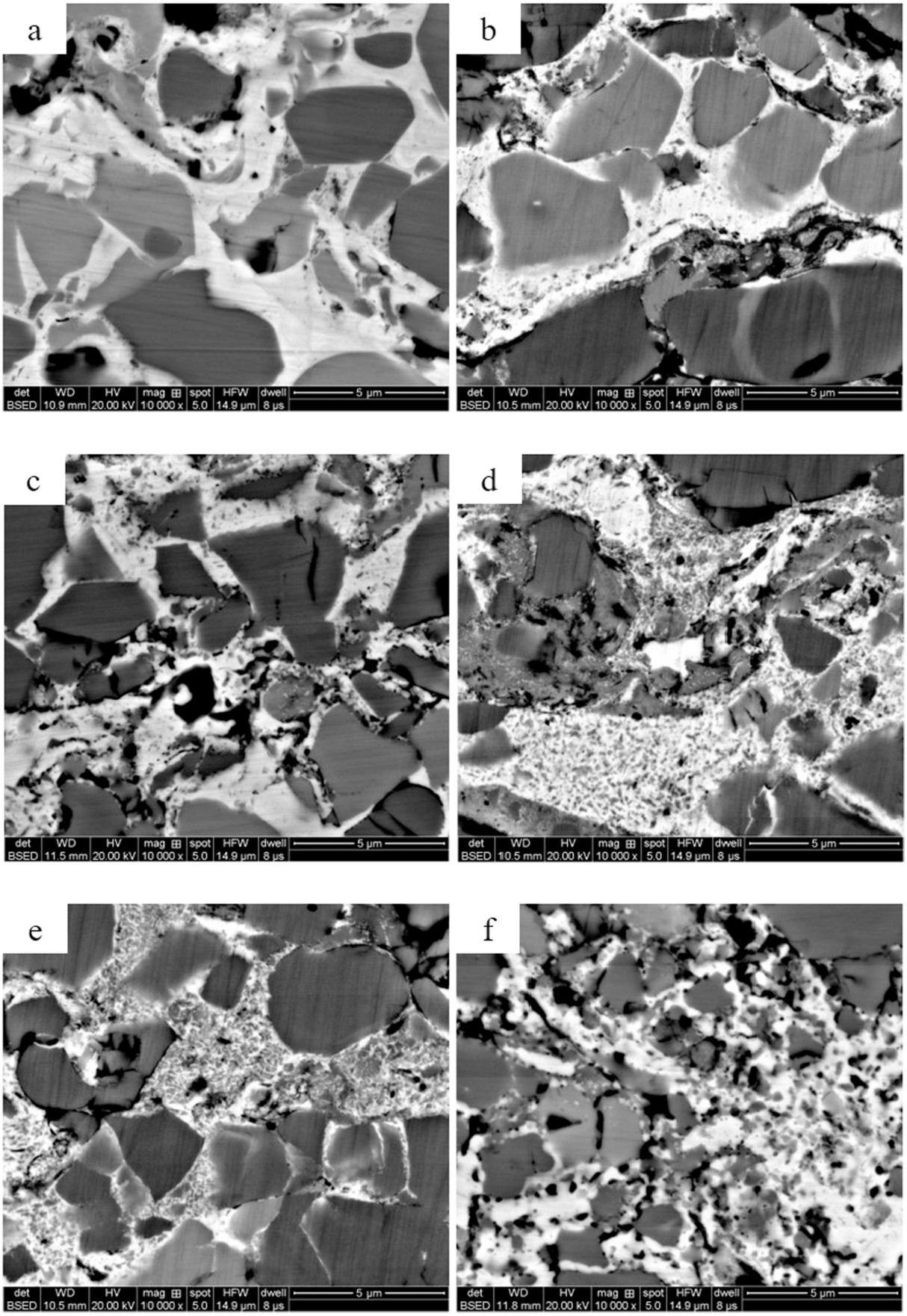

Fig. 12. The precipitation of secondary chromium carbides in remelted coating: (a) Remelting power at 30 kW (RP30), (b) Remelting power at 33 kW (RP33), (c) Remelting power at 36 kW (RP36), (d) Remelting power at 39 kW (RP39), (e) Remelting power at 42 kW (RP42), (f) Remelting power at 45 kW (RP45).

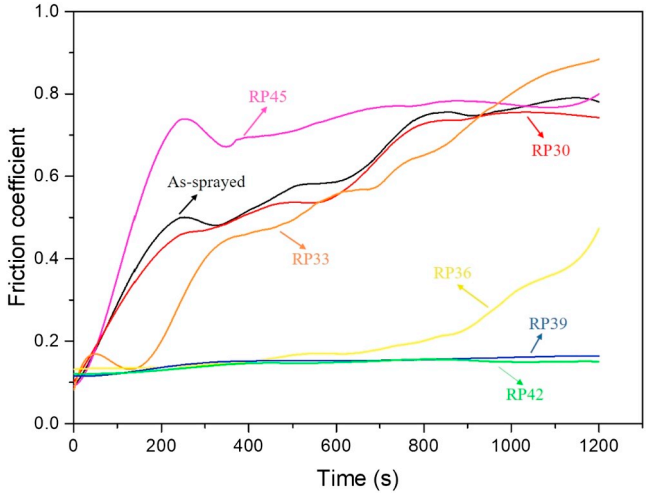

Fig. 13. Friction coefficient of plasma remelted coating.

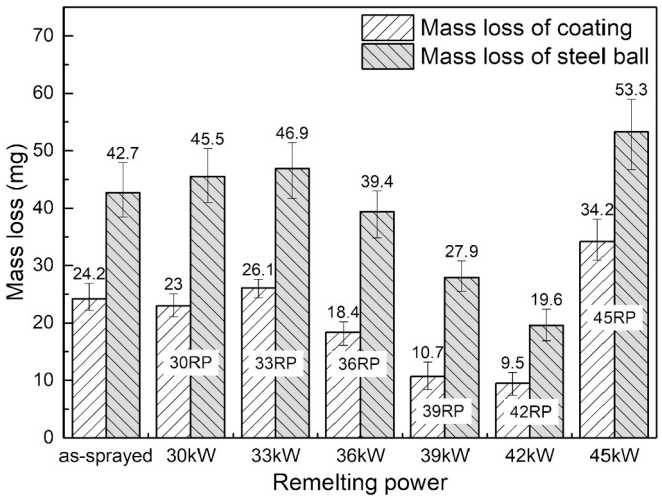

Fig. 14. Mass loss of as-sprayed and plasma remelted coatings.

boundary between the bond layer and the substrate is relatively clear, and a small amount of pores and cracks exist near the interface. In addition, no obvious microstructure change has been observed at the interface compared with the original coating. Both the amount and dimension of pores are increased for the coating remelted at 45 kW (Fig. 8(b)). The bonding layer is evidently delaminated from the substrate, which adversely affects the combination of the coating and the substrate.

The enhancement of coating-substrate bonding strength is probably caused by the heating effect of the plasma jet on the coating surface, and this incidence may lead to element diffusion in the coating material and a metallurgical union may have taken place [32]. Element diffusion near the interface can be observed by EDS line scanning. Since the scanning results of RP30, RP33, RP36 are similar, RP36, RP39, RP42 and RP45 coatings are selected for analysis by energy spectrometer. The results are shown in Fig. 9.

As shown in Fig. 9 (a), the “steep cliff” changes of Ni, Cr, Fe and other elements are observed at the functional-bonding and bonding-substrate interfaces for RP36 coating. No apparent element diffusion happened near two interfaces, and the mechanical joining is the main bonding mechanism. In contrast, weak element diffusion can be found in the 39 kW remelted coating at the functional–bonding interface, but the diffusion phenomenon is not obvious, as shown in Fig. 9(b). As the remelting power increases to 42 kW, slight quantitative changes of the elements such as Ni and Cr take place near the functional–bonding interface, as shown in Fig. 9(c). It is suggested that thermal diffusion of elements occurs near the interface due to the increase of the thermal input. It is indicated that the bonding mechanism between the functional layer and bonding layer is not only mechanical but also slightly metallurgical. This bonding mode is more solid than pure mechanical mode which reinforces the adhesion of the coating. However, the bonding mode between the bonding layer and substrate is still mainly mechanical according to the line scanning. In the coating remelted with 45 kW power (in Fig. 9(d)), the compositional gradient is less sharp, which indicates both thermal diffusion and metallurgical bonding are strengthened. Nevertheless, delamination is observed between the bonding layer and substrate.

3.3. Coating hardness analysis

In Fig. 10, the average values of microhardness are plotted in relation to the distance from the substrate interface (0 represents the interface), for plasma remelted Cr_3C_2-NiCr/NiCrAl coatings with different remelting powers. As the distance increases, the microhardness increases sharply at 150 μm. This is mainly due to the microhardness of the functional layer being much higher than the bonding layer. In addition, the microhardness values are improved significantly with the increased remelting power up to 42 kW, which is partly attributed to the decrease of porosity and the increase of density, as shown in Fig. 11. Besides, the increase of hardness of the remelted coatings may also be due to secondary carbides since the precipitation of secondary chromium carbides from the NiCr binder phase is driven by the heat input of the plasma arc [14,33]. As shown in Fig. 12(d) and (e), plasma remelting at 39 kW and 42 kW leads to a mass of secondary carbides in the binder matrix, the start of Ostwald ripening is evident as first agglomerations of secondary and primary carbides, similar phenomena have been reported in some literature sources [22,34,35]. However, with the continuous rise of remelting power, the microhardness of the RP45 coating decreases and the porosity of coating increases. A steep temperature gradient is induced under the local high heat input during plasma remelting. Further, the residual stress is increased due to the quick heating and quenching process, which leads to the increase in the amount of cracks and the decrease of the density of the coating. On the other hand, microhardness values of coatings with different remelting powers are higher than that of the as-sprayed coating, which proves that plasma remelting can improve the coating hardness.

3.4. Sliding wear resistance

Friction and wear tests are conducted on the surfaces of Cr_3C_2-NiCr/NiCrAl coatings with different remelting powers, and the non-remelted coating is set as the control. The measured friction coefficient curves after smoothing are shown in Fig. 13, and the mass losses of as-sprayed and plasma remelted coatings are compared in Fig. 14.

The trend of friction coefficient curves of the RP30, RP33 coatings and the as-sprayed coating are similar. As the friction coefficient stabilized, the friction coefficients of RP30, RP33 and as-sprayed coating are 0.811, 0.734 and 0.879 respectively. It is shown that the differences among the sliding wear responses of the RP30, RP33 coating and the as-sprayed coating are not significant. Similarly, the mass losses of the as-sprayed, RP30 and RP33 remelted coatings are at the same level, recorded as 24.2 mg, 23 mg and 26.1 mg, and the mass loss of counterpart steel balls has no obvious changes. When the remelting power increases to 36 kW, the friction coefficient of the coating is significantly

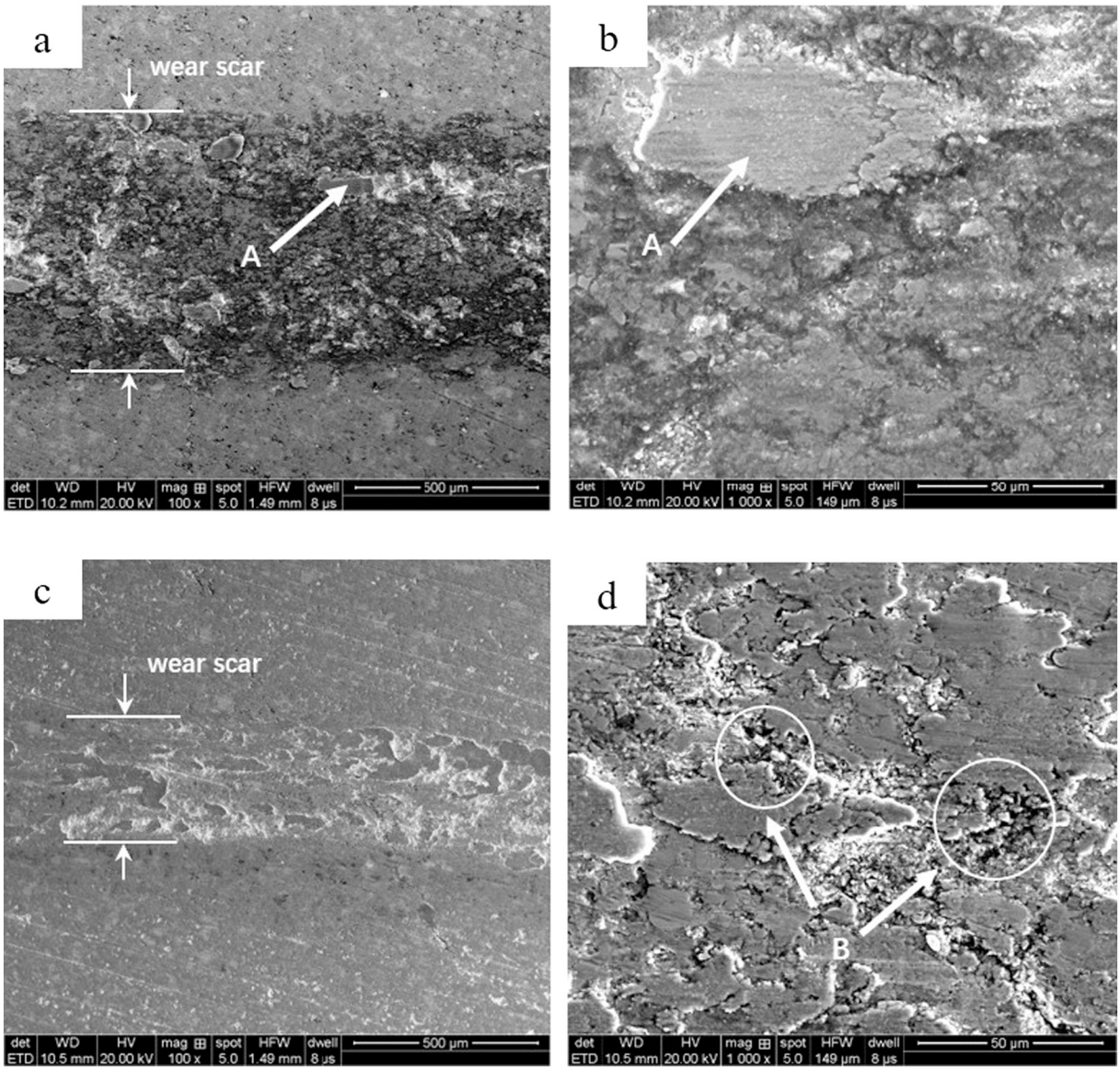

Fig. 15. Morphology of wear scars on coating surfaces: (a) Plasma remelting at 33 kW (RP33-200×), (b) Plasma remelting at 33 kW (RP33-1000×), (c) Plasma remelting at 36 kW (RP36-200×), (d) Plasma remelting at 36 kW (RP36-1000×), (e) Plasma remelting at 42 kW (RP42-200×), (f) Plasma remelting at 42 kW (RP42-1000×), (g) Plasma remelting at 45 kW (RP45-200×), (h) Plasma remelting at 45 kW (RP45-1000×).

decreased after 10 min, and then the friction coefficient ends at 0.464. The mass loss of RP36 coating and steel ball are 18.4 mg and 39.4 mg respectively, which indicates that sliding wear resistance of the RP36 coating is improved compared with the as-sprayed coating and the mass loss of steel balls decreases. By contrast, the friction coefficients of RP39 and RP42 only increase slightly during the initial stage of the test, then tend to be stable and keep at lower values compared with the other specimens. The mass losses of the RP39 and RP42 coating are 10.7 mg and 9.5 mg respectively: the values are lower than those of the other coatings. And the mass loss of their counterparts (steel balls) decreases evidently, which indicates that the plasma remelting at 39 kW and 42 kW improves the sliding wear resistance of coatings. The best sliding wear resistance is achieved with a remelting power of 42 kW. However, the friction coefficient of the RP45 coating presents a sharp rise at the early stage and then stabilizes at 0.788. The mass losses of the RP45 coating and steel ball are 34.2 mg and 53.3 mg. Noticeably, the friction coefficient of the coating is higher than that of the as-sprayed coating during the friction and wear tests, so the sliding wear response of the RP45 coating is degraded, which leads to the generation of rough surfaces and the increase of counterpart steel balls' wear.

The surface morphologies of the worn coatings and the element distributions have been examined by SEM and EDS. RP33, RP36, RP42 and RP45 coatings are selected for analysis as shown in Fig. 15.

As shown in Fig. 15(a) and (b), evident wear scars appear on the surface of the RP33 coating. Under the action of cyclic load, there is a large number of chromium carbide hard phase and the nickel chrome adhesive phase peeling on the coating surface, and the exfoliated particles become abrasive particles in the process of friction. Gray patches of different sizes appear on the wear scar of the RP33 coating (as indicated by the arrow A). Adhesive wear appears on the surface wear scar, and the main content of adhesions mainly is iron according to the EDS spectrum (in Fig. 16(a) and (b)), which is caused by wear of the

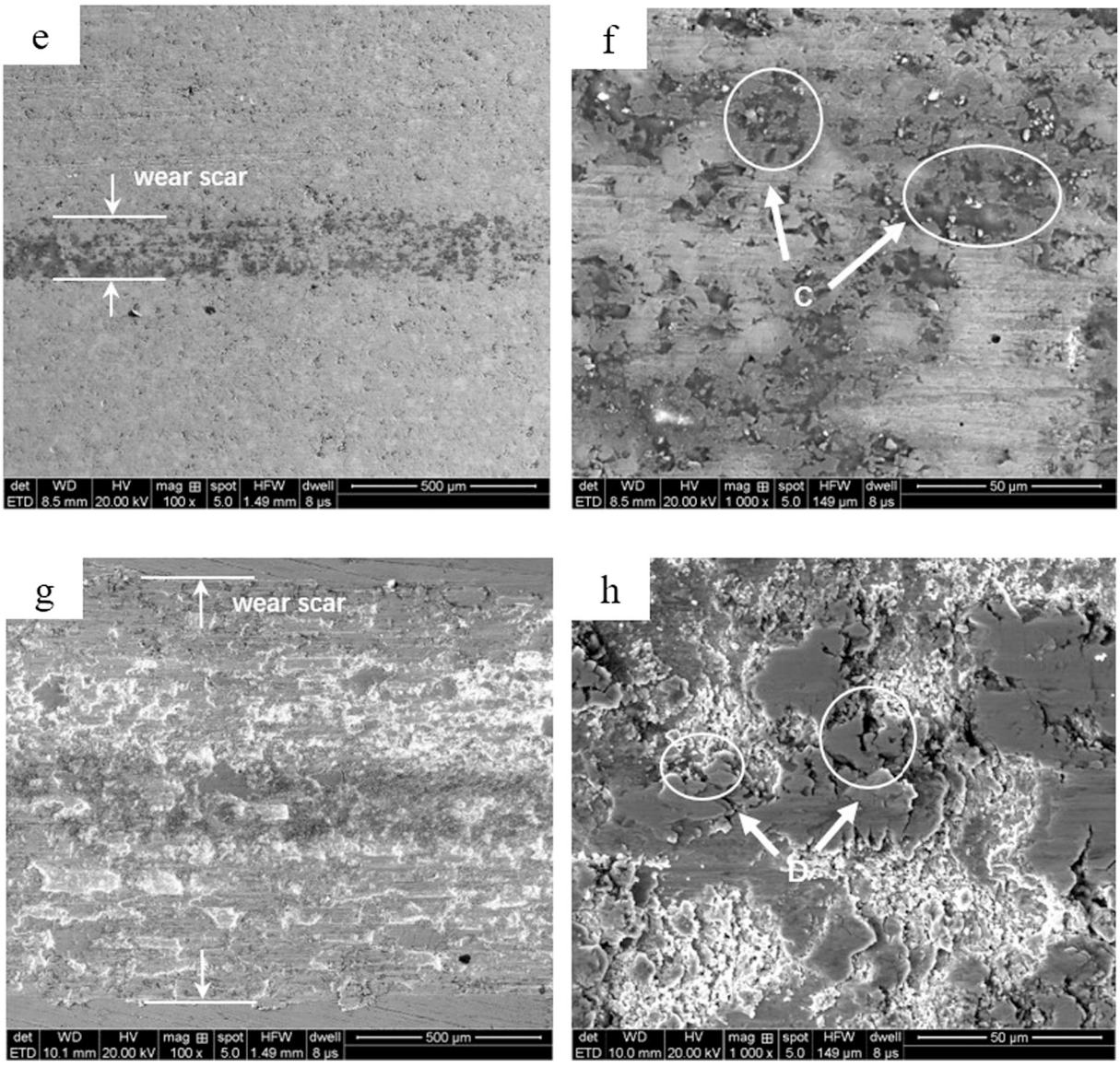

Fig. 15. (*continued*)

steel ball, and the formation of wear debris attached to the uneven coating surface. According to Fig. 16(c) and (d), the main element contents on the RP36 coating of point 1 and 2 are basically the same, especially chromium, nickel and carbon, while point 3 (shown in Fig. 16(d)) is the unworn area (not in the wear scar). Combined with XRD test results, it can be concluded that the dark part of the wear scar and the outer (unworn) coating surface mainly consist of Cr_3C_2 and NiCr. The wear mechanisms of coating of abrasive wear and adhesive wear. As can be seen from Fig. 15(c) and (d), the wear scar on the surface of the RP36 coating tends to be narrower and shallower, which indicates that the sliding wear loss of the remelted coating decreases as the remelting power increases to 36 kW. The surface oxide film is crushed by the tip of the iron ball (as shown in arrow B) due to effect of cycle loading. Crack initiation and spread appear on the coating surface and white bright band is the sharp edges of surface oxidation film after peeling. Therefore, the main wear pattern of coating is flake oxide film peeling. In Fig. 15(e) and (f), the wear scar on the surface of the RP42 coating is inconspicuous and the RP42 coating shows better sliding wear resistance compared to the other remelted coatings. A small number of white dots are iron based particles remaining on the coating surface after friction according to EDS spectra (in Fig. 17). During the wear process, the softer NiCr bonding phase in the coating will stick off (as indicated by arrow C), which shows typical adhesive wear, and the chromium carbide hard phase remains on the surface of the coating to prevent the further wear. Notably, the most evident wear scar can be observed on the RP45 coating surface (in Fig. 15(g) and (h)). The width of wear scar increases. Dark bands appear in the middle of the wear scar due to grinding between coating and tip of the iron ball. The surface of the RP45 coating is delaminated and spalled after friction (as shown in the arrow D) and the surface oxide film of the coating is peeling off and the exposed fresh surface is also worn and damaged. The bright white area is caused by the spalling of the coating lamellar structure and the spalling particles become abrasive particles in the friction process and aggravate the wear. Therefore, the main wear pattern of the coating is the wear of abrasive particles and brittle fracture caused by the spalling of oxide film and coating.

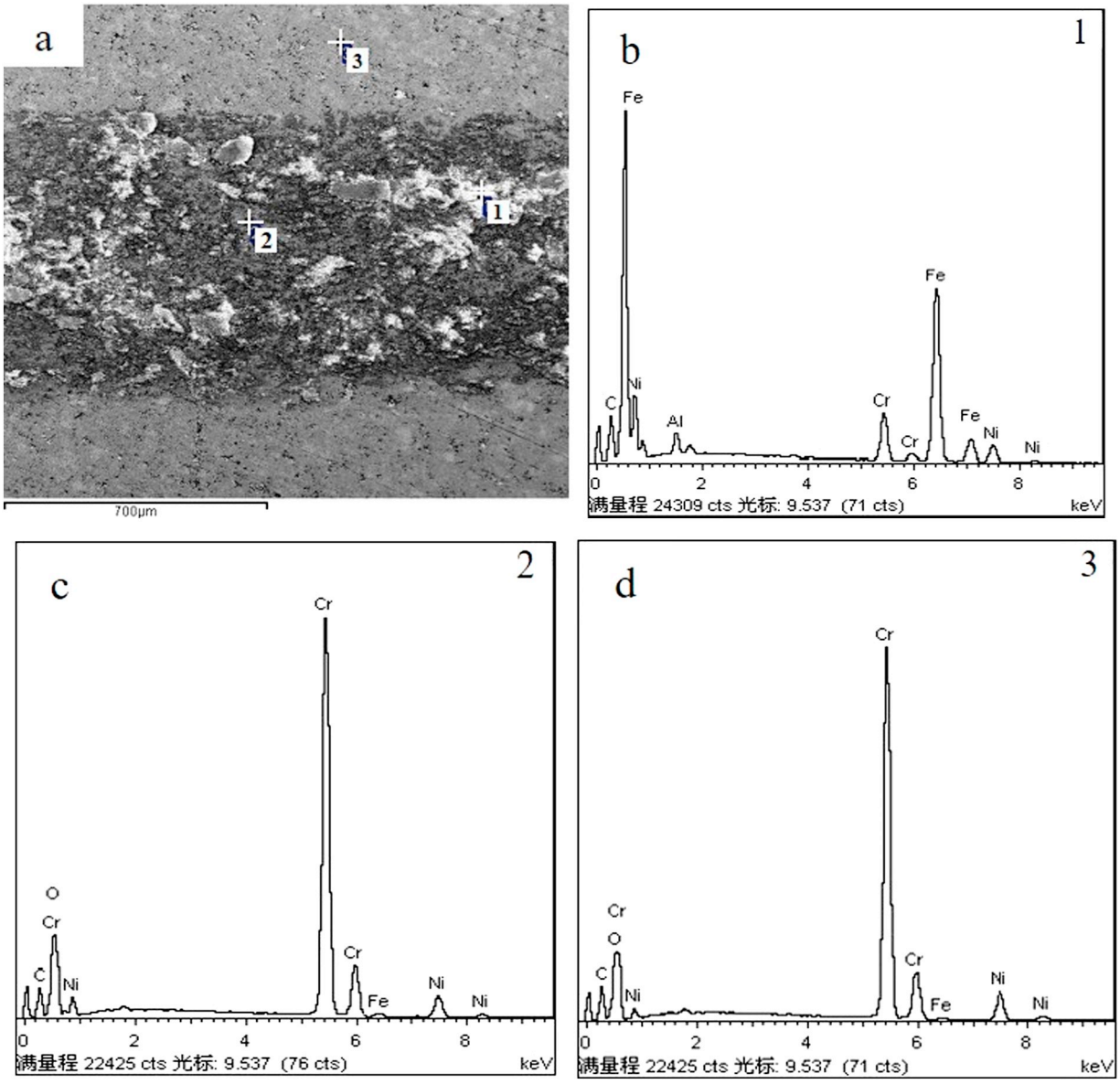

Fig. 16. EDS micrographs of RP33 wear scar: (a) SEM image showing the positions of points 1, 2, 3, (b) corresponding EDS spectra.

4. Conclusions

The microstructure and properties of Cr_3C_2-NiCr/NiCrAl coatings on FV520B steel substrates after plasma arc remelting have been investigated The effects of remelting powers on the microstructure and phase composition, bonding strength and hardness, and the porosity and wear resistance of the coatings are experimentally studied and the associated mechanism are analyzed in detail. The proper usage of plasma arc remelting is an effective approach to enhance the properties of the thermal sprayed Cr3C2-NiCr/NiCrAl composite coating. The following conclusions are obtained.

1. The remelted coating is mainly composed of Cr_3C_2, (Cr, Ni), $Cr_{23}C_6$, and Cr_2O_3 phases, where $Cr_{23}C_6$ and Cr_2O_3 are increased compared with the as-sprayed coating. With the increase of remelting power to 42 kW, the porosity and microcracks of the coating are reduced to a minimum since the NiCr metallic phase is melted and filled into the porosity and microcracks.
2. Plasma arc remelting promotes element diffusion across the interface between the functional and bonding layer, the coating adhesion is improved due to partial metallurgical combination at suitable remelting power. Nevertheless, remelting with excessive power results in delamination between the bonding layer and substrate, which has adverse effect on the coating adhesion.
3. The microhardness of coatings remelted with different power levels increases compared with that of the as-sprayed coating, which is caused by increase of density and precipitation of secondary carbides.
4. Plasma arc remelting with appropriate power can enhance the sliding wear resistance of the coating, but excessive heat input (above 42 kW) increases the sliding wear loss of the coating.

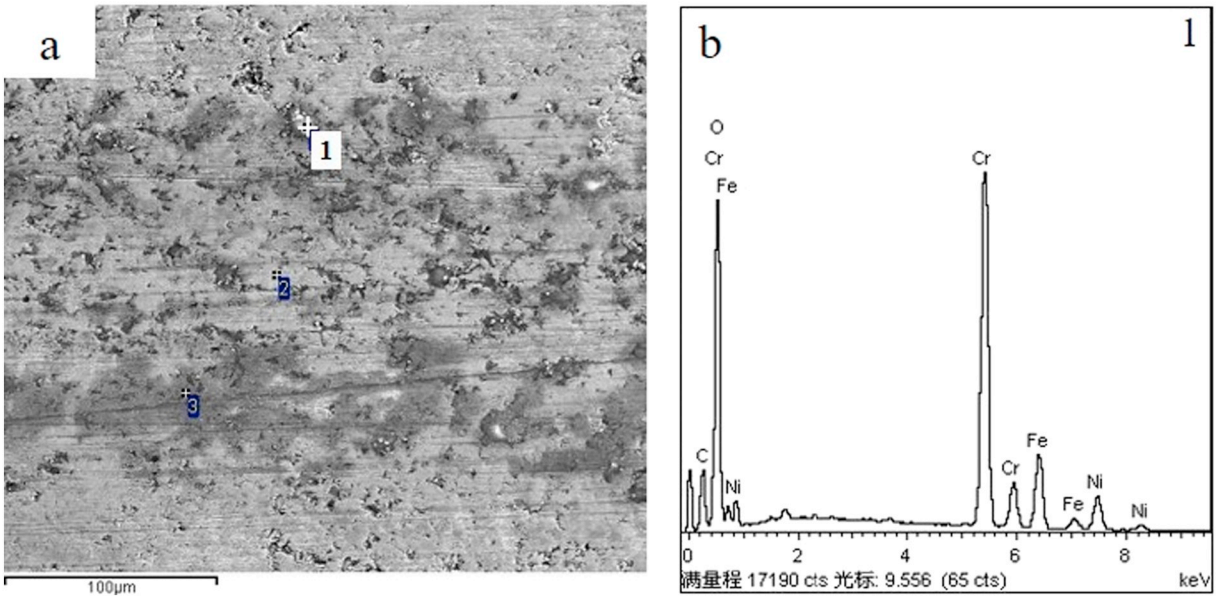

Fig. 17. EDS micrographs of RP42 wear scar: (a) SEM image showing the positions of points 1, (b) corresponding EDS spectra.

Acknowledgements

This work was funded by NSFC (51605258) and Major scientific and technological innovation projects of Shandong (2018CXG0807) to carry out this research work.

References

[1] M. Cekada, P. Panjan, M. Maček, P. Šmíd, Comparison of structural and chemical properties of Cr-based hard coatings, Surf. Coatings Technol. 151–152 (2002) 31–35, https://doi.org/10.1016/S0257-8972(01)01582-1.
[2] G. fang Sun, Y. kang Zhang, C. sheng Liu, K. yu Luo, X. qi Tao, P. Li, Microstructure and wear resistance enhancement of cast steel rolls by laser surface alloying NiCr-Cr3C2, Mater. Des. 31 (2010) 2737–2744, https://doi.org/10.1016/j.matdes.2010.01.021.
[3] S. Matthews, B. James, M. Hyland, High temperature erosion-oxidation of Cr3C2-NiCr thermal spray coatings under simulated turbine conditions, Corros. Sci. 70 (2013) 203–211, https://doi.org/10.1016/j.corsci.2013.01.030.
[4] M. Roy, A. Pauschitz, J. Wernisch, F. Franek, The influence of temperature on the wear of Cr3C2-25(Ni20Cr) coating - comparison between nanocrystalline grains and conventional grains, Wear 257 (2004) 799–811, https://doi.org/10.1016/j.wear.2004.05.001.
[5] D. Poirier, J.G. Legoux, R.S. Lima, Engineering HVOF-sprayed Cr3C2-NiCr coatings: the effect of particle morphology and spraying parameters on the microstructure, properties, and high temperature wear performance, J. Therm. Spray Technol. 22 (2013) 280–289, https://doi.org/10.1007/s11666-012-9833-3.
[6] H.S. Sidhu, B.S. Sidhu, S. Prakash, Mechanical and microstructural properties of HVOF sprayed WC-Co and Cr 3C2-NiCr coatings on the boiler tube steels using LPG as the fuel gas, J. Mater. Process. Technol. 171 (2006) 77–82, https://doi.org/10.1016/j.jmatprotec.2005.06.058.
[7] S. Shrivastava, R. Upadhyaya, Study of fracture toughness and bend test morphologies of HVOF sprayed Cr3C2-25% NiCr coating after heat treatment, IOP Conf. Ser. Mater. Sci. Eng. 346 (2018), https://doi.org/10.1088/1757-899X/346/1/012026.
[8] L.M. Berger, Application of hardmetals as thermal spray coatings, Int. J. Refract. Met. Hard Mater. 49 (2015) 350–364, https://doi.org/10.1016/j.ijrmhm.2014.09.029.
[9] T. Sahraoui, N.E. Fenineche, G. Montavon, C. Coddet, Structure and wear behaviour of HVOF sprayed Cr3C2-NiCr and WC-Co coatings, Mater. Des. 24 (2003) 309–313, https://doi.org/10.1016/S0261-3069(03)00059-1.
[10] M. Akhtari Zavareh, A.A.D.M. Sarhan, B.B. Razak, W.J. Basirun, The tribological and electrochemical behavior of HVOF-sprayed Cr3C2-NiCr ceramic coating on carbon steel, Ceram. Int. 41 (2015) 5387–5396, https://doi.org/10.1016/j.ceramint.2014.12.102.
[11] N. Vashishtha, S.G. Sapate, Sliding wear maps for high velocity oxy fuel (HVOF) sprayed WC-12Co and Cr3C2 – 25NiCr coatings, Tribol. Int. 114 (2017) 290–305, https://doi.org/10.1016/j.triboint.2017.04.037.
[12] L. Janka, J. Norpoth, S. Eicher, M. Rodríguez Ripoll, P. Vuoristo, Improving the toughness of thermally sprayed Cr3C2-NiCr hardmetal coatings by laser post-treatment, Mater. Des. 98 (2016) 135–142, https://doi.org/10.1016/j.matdes.2016.03.007.
[13] B. Prawara, H. Yara, Y. Miyagi, T. Fukushima, Spark plasma sintering as a post-spray treatment for thermally-sprayed coatings, Surf. Coatings Technol. 162 (2003) 234–241, https://doi.org/10.1016/S0257-8972(02)00564-9.
[14] J. Mateos, J.M. Cuetos, E. Fernández, R. Vijande, Tribological behaviour of plasma-sprayed WC coatings with and without laser remelting, Wear 239 (2000) 274–281, https://doi.org/10.1016/S0043-1648(00)00325-2.
[15] S. Matthews, B. James, M. Hyland, The role of microstructure in the mechanism of high velocity erosion of Cr3C2-NiCr thermal spray coatings: part 2 - heat treated coatings, Surf. Coatings Technol. 203 (2009) 1094–1100, https://doi.org/10.1016/j.surfcoat.2008.10.013.
[16] S. Matthews, M. Bjames, Hyland, The effect of heat treatment on the oxidation mechanism of blended powder Cr3C2-NiCr coatings, Proc. Int. Therm. Spray Conf, vol. 19, 2009, pp. 1018–1023, , https://doi.org/10.1361/cp2009itsc1018.
[17] J.A. Picas, M. Punset, S. Menargues, M. Campillo, M.T. Baile, A. Forn, The Influence of Heat Treatment on Tribological and Mechanical Properties of HVOF Sprayed CrC–NiCr Coatings, vol. 2, Light Alloys and Surface Treatments Design Centre (CDAL). Technical University of Catalonia, 2009, pp. 225–228, https://doi.org/10.1007/s12289-009-0466-0.
[18] J. Iwaszko, Z. Nitkiewicz, Solidification microstructure of plasma sprayed and re-melted carbide coatings (Cr3C2/Ni-Al, W2C-WC/Co), Mater. Manuf. Process. 17 (2002) 169–176, https://doi.org/10.1081/AMP-120003527.
[19] W. Acchar, U.U. Gomes, W.A. Kaysser, J. Goring, Strength degradation of a tungsten carbide-cobalt composite at elevated temperatures, Mater. Charact. 43 (1999) 27–32, https://doi.org/10.1016/S1044-5803(98)00056-4.
[20] D.A. Stewart, P.H. Shipway, D.G. McCartney, Influence of heat treatment on the sliding wear behaviour of HVOF sprayed WC-Co coatings, Surf. Coatings Technol. 105 (1998) 13–24, https://doi.org/10.1016/S0257-8972(98)00444-7.
[21] E. Gruzdys, Š. Meškinis, S. Tamulevičius, T. Grinys, Effects of heating by arc discharge on structure and chemical composition of coatings formed using high velocity oxygen fuel and flame spraying processes, Medziagotyra 14 (2008) 234–237.
[22] L. Janka, J. Norpoth, R. Trache, L.M. Berger, Influence of heat treatment on the sliding wear resistance of a Cr3C2NiCr coating deposited by an ethene-fuelled HVOF spray process, Surf. Coatings Technol. 291 (2016) 444–451, https://doi.org/10.1016/j.surfcoat.2016.02.066.
[23] J. Morimoto, Y. Sasaki, S. Fukuhara, N. Abe, M. Tukamoto, Surface modification of Cr3C2-NiCr cermet coatings by direct diode laser, Vacuum 80 (2006) 1400–1405, https://doi.org/10.1016/j.vacuum.2006.01.070.
[24] Y. Fu, A.W. Batchelor, H. Xing, Y. Gu, Wear behaviour of laser-treated plasma-sprayed ZrO2coatings, Wear 210 (1997) 157–164, https://doi.org/10.1016/S0043-1648(97)00058-6.
[25] A.B. Murphy, D. Uhrlandt, M. Capitelli, L.D. Pietanza, Arc Welding, Plasma Cutting and Plasma, (2013), https://doi.org/10.1088/0022-3727/46/22/220301.
[26] K. Salonitis, S. Vatousianos, Experimental investigation of the plasma arc cutting process, Procedia CIRP 3 (2012) 287–292, https://doi.org/10.1016/j.procir.2012.07.050.
[27] L.A. Baeva, M.V. Il'ichev, A.S. Tyuftyaev, G.A. Filippov, L.E. Shchukina, Influence of nitrogen in plasma-arc remelting on the structure and properties of stainless steel, Steel Transl 47 (2017) 827–829, https://doi.org/10.3103/S0967091217120026.
[28] G. Xie, Y. Lu, Z. He, B. Hu, K. Wang, X. Mo, Y. Wu, P. Lin, Microstructure and corrosion properties of plasma-sprayed NiCr-Cr3C2coatings comparison with different post treatment, Surf. Coatings Technol. 202 (2008) 2885–2890, https://doi.org/10.1016/j.surfcoat.2007.10.024.
[29] T.S. Sidhu, State of the Art of HVOF Coating Investigations, (2015), https://doi.org/10.4031/002533205787443908.
[30] S. Hong, Y. Wu, Q. Wang, G. Ying, G. Li, W. Gao, B. Wang, W. Guo, Surface & coatings technology microstructure and cavitation – silt erosion behavior of high-velocity oxygen – fuel (HVOF) sprayed Cr 3 C 2 – NiCr coating, Surf. Coat. Technol. 225 (2013) 85–91, https://doi.org/10.1016/j.surfcoat.2013.03.020.
[31] N. Espallargas, J. Berget, J.M. Guilemany, A.V. Benedetti, P.H. Suegama, Cr 3 C 2 – NiCr and WC – Ni thermal spray coatings as alternatives to hard chromium for

erosion – corrosion resistance, 202 (2008) 1405–1417, https://doi.org/10.1016/j.surfcoat.2007.06.048.
[32] J. Mateos, J.M. Cuetos, R. Vijande, E. Fernández, Tribological properties of plasma sprayed and laser remelted 75/25 Cr3C2/NiCr coatings, Tribol. Int. 34 (2001) 345–351, https://doi.org/10.1016/S0301-679X(01)00023-8.
[33] L. Janka, J.N.R. Trache, HVOF- and HVAF-sprayed Cr 3 C 2-NiCr coatings deposited from feedstock powders of spherical morphology: microstructure formation and high-stress abrasive wear resistance up to 800° C, J. Therm. Spray Technol. 26 (2017) 1720–1731, https://doi.org/10.1007/s11666-017-0621-y.
[34] J.K.N. Murthy, S. Bysakh, K. Gopinath, B. Venkataraman, Microstructure dependent erosion in Cr 3 C 2 – 20 (NiCr) coating deposited by a detonation gun, 202 (2007) 1–12, https://doi.org/10.1016/j.surfcoat.2007.03.017.
[35] F. Otsubo, H. Era, T. Uchida, K. Kishitake, Properties of Cr 3 C 2 -NiCr Cermet Coating Sprayed by High Power Plasma and High Velocity Oxy-Fuel Processes, vol. 9, (2000), pp. 499–504.